Calcium-Dependent and -Independent Interactions of the Calmodulin-Binding Domain of Cyclic Nucleotide Phosphodiesterase with Calmodulin†

Tao Yuan,‡ Michael P. Walsh,§ Cindy Sutherland,§ Heinz Fabian,|| and Hans J. Vogel*,‡

Structural Biology Research Group, Department of Biological Sciences, and Smooth Muscle Research Group, Department of Biochemistry and Molecular Biology, University of Calgary, 2500 University Drive, N.W., Calgary, Alberta, Canada T2N 1N4, and Max-Delbrück-Center for Molecular Medicine, Robert-Rössle-Strasse, D-13125 Berlin, Germany

Received July 9, 1998; Revised Manuscript Received October 30, 1998

ABSTRACT: The ubiquitous Ca^{2+}-binding regulatory protein calmodulin (CaM) binds and activates a wide range of regulatory enzymes. The binding is usually dependent on the binding of Ca^{2+} to CaM; however, some target proteins interact with CaM in a calcium-independent manner. In this work, we have studied the interactions between CaM and a 20-residue synthetic peptide encompassing the major calmodulin-binding domain of cyclic nucleotide phosphodiesterase (PDE1A2). The binding was studied in the absence and presence of Ca^{2+} by far-UV and near-UV circular dichroism, fluorescence, and infrared spectroscopy. In addition, two-dimensional heteronuclear NMR studies with ^{13}C-methyl-Met-CaM and uniformly ^{15}N-labeled CaM were performed. Competition assays with smooth muscle myosin light chain kinase revealed a K_d of 224 nM for peptide binding to Ca^{2+}-CaM, while binding of the peptide to apo-CaM is weaker. The peptide binds with an α-helical structure to both lobes of Ca^{2+}-saturated CaM, and the single Trp residue is firmly anchored into the C-terminal lobe of CaM. In contrast, the Trp residue plays a minor role in the binding to the apo-protein. Moreover, when bound to apo-CaM, the PDE peptide is only partially helical, and it interacts solely with the C-terminal lobe of CaM. These results show that the Ca^{2+}-induced activation of PDE involves a significant change in the structure and positioning of the CaM-bound PDE peptide domain.

Calmodulin (CaM)[1] is the most important Ca^{2+}-binding regulatory protein in eukaryotic cells. It can bind and activate more than 40 different target proteins, including protein kinases, phosphatase 2B (calcineurin), nitric oxide synthases, cyclic nucleotide phosphodiesterases, various actin-binding proteins, ion channels, etc. (for reviews, see refs *1*−*4*). In the absence or presence of four Ca^{2+} ions, CaM adopts a dumbbell-shaped structure with two lobes connected by a 26-residue central linker region (*5*−*7*). Each lobe of CaM contains two "helix-loop-helix" Ca^{2+}-binding motifs connected by a small β-sheet between the two Ca^{2+}-binding loops. Although the central linker region of Ca^{2+}-CaM is an α-helix in the crystal structure (*5*), nuclear magnetic resonance (NMR) spectroscopy indicated that the central part of the linker region is unstructured in solution (*8*). The majority of the hydrophobic residues in apo-CaM are buried or partially buried inside the protein (*6*, *7*). Upon binding four Ca^{2+} ions, CaM experiences significant movements among α-helices in each lobe and the interhelix angles change dramatically (*6*, *7*). As a result, Ca^{2+} binding exposes one Met-rich hydrophobic patch on each lobe of CaM for target protein binding (*5*). The CaM-binding domains in target proteins usually comprise a stretch of ∼20 amino acid residues with the potential to form a basic amphipathic α-helix (*9*). High-resolution structures of Ca^{2+}-CaM complexed with binding domain peptides from two target proteins revealed that the CaM-binding peptides bind to Ca^{2+}-CaM as α-helices, and that side-chain hydrophobic interactions between the peptide and Ca^{2+}-CaM provide the dominant force in the binding (*10*−*12*). It is generally believed that the flexible central linker region and the two Met-rich hydrophobic patches are important features for CaM's versatility. The flexible central linker region can unwind to different extents to accommodate the binding of distinct target proteins, while the Met residues of the two hydrophobic patches in Ca^{2+}-CaM provide a highly adjustable

† This work was supported by operating grants from the Medical Research Council of Canada (MRC) to H.J.V. (MT-9673) and M.P.W. (MT-13101). T.Y. holds a Studentship from the Alberta Heritage Foundation for Medical Research (AHFMR). H.J.V. and M.P.W. are AHFMR Medical Scientists. The NMR spectrometer used in this study has been funded and maintained with funds provided by AHFMR and MRC.

* To whom correspondence should be addressed. Tel: (403) 220-6006. Fax: (403) 289-9311. E-mail: vogel@ucalgary.ca.

‡ Structural Biology Research Group, University of Calgary.

§ Smooth Muscle Research Group, University of Calgary.

|| Max-Delbrück-Center for Molecular Medicine.

[1] Abbreviations: 2D, two-dimensional; CaM, calmodulin; CaMKI, calmodulin-dependent protein kinase I; CaMKII, calmodulin-dependent protein kinase II; CD, circular dichroism; COSY, correlated spectroscopy; CT-CaM, a CaM mutant with four Met residues in the C-lobe of CaM (M109, M124, M144, and M145) mutated to Leu residues; FTIR, Fourier transform infrared; HMQC, heteronuclear multiple quantum coherence; HSQC, heteronuclear single quantum coherence; NMR, nuclear magnetic resonance; NOESY, nuclear Overhauser effect spectroscopy; PDE, cyclic nucleotide phosphodiesterase; SeMet, selenomethionine; SeMet-CaM, a CaM variant with nine Met residues substituted by the unnatural amino acid selenomethionine; SeMet-CT-CaM, a CT-CaM with the remaining five Met residues substituted by the unnatural amino acid selenomethionine; smMLCK, smooth muscle myosin light chain kinase; TFE, trifluoroethanol; TOCSY, total correlation spectroscopy.

10.1021/bi9816453 CCC: $18.00
Published on Web 01/15/1999

hydrophobic surface for binding due to the intrinsic flexibility of the Met side chain and the high polarizability of the sulfur atom in Met residues (*13*).

Cyclic nucleotide phosphodiesterase (PDE) belongs to a family of enzymes whose function is to terminate cyclic nucleotide second messenger signaling (*14*). Seven different classes of PDE have been identified to date, and the first subfamily, PDE1, preferentially hydrolyses cAMP and is activated by Ca^{2+} and CaM. The CaM-binding domain is located in the N-terminal part of PDE1 (*15, 16*); for PDE1A2 (brain 61 kDa isozyme) it corresponds to the residues 23−41 (*15*). PDE has frequently been used to assess the effects of mutations in CaM on enzyme activation, yet the details of the interaction between CaM and PDE remain to be clarified.

Here we have studied a synthetic peptide encompassing the CaM-binding domain of PDE1A2 (referred to as the PDE peptide), and its interaction with CaM. Competition assays with smooth muscle myosin light chain kinase (smMLCK) as well as circular dichroism (CD), Fourier transform infrared (FTIR), fluorescence, and NMR spectroscopy were performed. We found that the PDE peptide binds to Ca^{2+}-CaM with an α-helical structure and in doing so effectively inhibits the activation of smMLCK. In the absence of Ca^{2+}, the PDE peptide binds to apo-CaM also as an α-helix with some β-turn structure. The C-terminal lobe of apo-CaM provides the major binding site for the PDE peptide, while it binds to both lobes of Ca^{2+}-CaM. Moreover, the PDE peptide binds to Ca^{2+}-CaM in an antiparallel orientation, similar to the CaM-binding domain peptides derived from MLCK and CaM-dependent protein kinase II (CaMKII) (*10*−*12*).

MATERIALS AND METHODS

Materials. [γ-^{32}P] ATP (>5000 Ci/mmol) was purchased from Amersham Corp. (Oakville, Ontario, Canada). Bovine CaM was purified from bovine brain (*17*). MLCK was purified from chicken gizzard smooth muscle (*18*). CaM used for spectroscopic studies was cloned and overexpressed in *Escherichia coli* and purified as described (*19*). Carbon-13 methyl-Met-labeled CaM, uniformly ^{15}N-labeled CaM, and uniformly ^{13}C/^{15}N-labeled CaM were purified following published procedures (*20, 21*). The other CaM variants (CT-CaM, SeMet-CaM, and SeMet-CT-CaM) were purified as described (*22*). The PDE peptide was commercially synthesized in the Protein and DNA Synthesis Facility at Queen's University, Kingston, Ontario, Canada. The MLC_{11-23} peptide was synthesized in the Peptide Synthesis Facility at the University of Calgary, Calgary, Alberta, Canada. The purity of the peptides was confirmed by analytical high-pressure liquid chromatography, amino acid analysis, and mass spectrometry. The sequences of these peptides are (i) MLC_{11-23} (KKRPQRATS^{19}NVFA), an MLCK substrate corresponding to residues 11−23 of the 20 kDa light chain of chicken gizzard myosin, Ser19 being the site of phosphorylation by MLCK (*23*); and (ii) the PDE peptide (Ac-QTEKMWQRLKGILRCLVKQL-NH_2), corresponding to the CaM-binding domain of bovine brain PDE1A2 (*15, 24*).

MLCK Assays. MLCK activity was measured at 30 °C under the following conditions: 20 mM Tris-HCl, pH 7.5, 60 mM KCl, 4 mM $MgCl_2$, 0.2 mM $CaCl_2$, 0.2 mM [γ-^{32}P]-ATP (~300 cpm/pmol), 0.1 mM MLC_{11-23}, 0−400 nM CaM, 10 nM MLCK, and varying concentrations of CaM-binding peptides. Reactions (30 μL) were started by the addition of ATP and quenched after 5 min by spotting 20 μL onto P81 phosphocellulose paper squares (Whatman) which were washed and counted as previously described (*25*). Phosphate incorporation into MLC_{11-23} was shown to be linear for at least 5 min. Maximal MLCK activity observed at 400 nM CaM was 0.44 ± 0.16 μmol of Pi incorporated min^{-1} (mg of MLCK)$^{-1}$ (mean of 28 independent measurements each carried out in triplicate, the standard deviation was always below 10% for each point). Basal MLCK activity in the absence of CaM was 0.08 ± 0.03 μmol of Pi incorporated min^{-1} (mg of MLCK)$^{-1}$ (mean of 30 independent measurements each carried out in triplicate).

The dissociation constant (K_d) of CaM for the PDE peptide was calculated from the midpoint of the activation curve of MLCK by CaM in the absence and presence of a known concentration of peptide using the following equation (*26*):

$$K_d = \frac{([P_t] + K - [CaM])K}{[CaM] - K}$$

where $[P_t]$ is the total concentration of peptide added, and K and [CaM] are the concentrations of CaM required to reach half-maximal activation in the absence and presence of peptide, respectively.

CD Spectroscopy. CD spectra were acquired on a Jasco J-715 spectropolarimeter in the Department of Chemistry, University of Calgary, Calgary, Alberta, Canada. All experiments were performed at ambient temperature (22 °C) using a 0.1 cm path length cylindrical quartz cuvette for the far-UV region and a 1 cm path length cylindrical quartz cuvette for the near-UV region. The parameters used are as follows: 0.2 nm step resolution, 50 nm/min speed, 2 s response time, 1 nm bandwidth. The sensitivity for the far-UV region is 20 mdeg, and the sensitivity for the near-UV region is 10 mdeg. Far-UV CD spectra were averaged over 10 scans, and near-UV CD spectra were the average of 20 scans. The concentration of CaM or peptide used for far-UV measurements was 10 μM in 10 mM Tris-HCl, pH 7.2, with 2 mM $CaCl_2$ or 2 mM EDTA, in a total volume of 200 μL. PDE peptide samples also contained 1 mM DTT to prevent any dimerization of the peptide due to the presence of a single Cys residue. The concentration of CaM or peptide used for near-UV measurement was 50 μM in 25 mM Tris-HCl, pH 7.2, 100 mM KCl, with 5 mM $CaCl_2$ or 5 mM EDTA, in a total volume of 2 mL. The background signals from the buffer were subtracted from each spectrum, and then each spectrum was smoothed and converted to molar ellipticity using Jasco software (near-UV CD spectra were not smoothed). The CD spectra were reported either as molar ellipticity or as mean residue molar ellipticity. The α-helical content of peptides was calculated according to Scholtz et al. (*27*).

FTIR Spectroscopy. For the infrared measurements, apo-CaM was dissolved in D_2O buffer (100 mM sodium cacodylate, pH 7) and left overnight at room temperature to ensure the complete exchange of all amide protons with deuterium. The Ca^{2+} form was then prepared by adding the appropriate amount of $CaCl_2$ to the apo-CaM solution. Infrared spectra were recorded on a Bruker IFS-66 FTIR spectrometer equipped with a DTGS detector and continu-

ously purged with dry air. The protein solutions were placed between a pair of CaF_2 windows separated by 50 μm at ambient temperature. For proper compensation of D_2O absorption, the buffer solutions were measured in a cell with a slightly shorter path length. If necessary, the protein spectra were corrected for residual water vapor using a set of water vapor spectra. For each sample, 256 interferograms were co-added and Fourier transformed to yield spectra with a nominal resolution of 4 cm^{-1}.

Fluorescence Spectroscopy. Steady-state Trp fluorescence was carried out on a Hitachi-2000 spectrofluorimeter as described (*22*). The Trp fluorescence was excited at 295 nm to reduce the excitation of the two Tyr residues of CaM. Emission wavelength profiles were collected from 300 to 450 nm. Fluorescence samples contained 10 μM PDE peptide in 10 mM Tris-HCl, pH 7.2, 100 mM KCl, 1 mM DTT in the presence of 1 mM $CaCl_2$ or 5 mM EDTA. The concentration of CaM used was 15 μM to ensure complete saturation of the PDE peptide (*28*). Samples were incubated at 37 °C for 2 h before the fluorescence measurements were made to ensure complete reduction of the peptide thiol.

NMR Spectroscopy. All NMR spectra were acquired on a Bruker AMX-500 spectrometer at 298 K. The sample of ^{13}C-methyl-Met-labeled CaM contained 0.6 mM apo-CaM, 100 mM KCl in 99.9% D_2O, pD 7.5 (not corrected for the isotope effects). Two-dimensional (2D) ^{1}H, ^{13}C heteronuclear multiple quantum coherence (HMQC) spectra were acquired as described (*29*). Quadrature detection in the F_1 dimension was obtained using the time-proportional phase incrementation technique. The sweep width was 6 ppm in both ^{1}H and ^{13}C dimensions with the ^{1}H carrier set at 500.1388 MHz and the ^{13}C carrier set at 125.7613 MHz. The sizes of the ^{1}H, ^{13}C HMQC spectra were 1024 × 128 real data matrix with 8 scans for each experiment. The sample of uniformly ^{15}N-labeled CaM contained 0.9 mM apo-CaM, 100 mM KCl in 90% H_2O, 10% D_2O, pH 6.3 (not corrected for the isotope effects). Two-dimensional ^{1}H, ^{15}N heteronuclear single quantum coherence (HSQC) spectra were acquired with a *z*-axis pulsed field gradient shielded triple resonance probe using a standard pulse sequence (*30*). The sweep width was 12 ppm in the ^{1}H dimension and 38 ppm in the ^{15}N dimension with the ^{1}H carrier at the H_2O frequency and the ^{15}N carrier at 50.6845 MHz. The water resonance was presaturated during the acquisition. The sizes of the ^{1}H, ^{15}N HSQC spectra were 2048 × 256 real data matrix with four scans for each experiment. Two-dimensional homonuclear proton NMR spectra were acquired for the spectral assignment of the PDE peptide in a 30% aqueous TFE solution. The peptide sample contained 1 mM PDE peptide in 30% TFE, 10% D_2O, and 60% H_2O, pH 5.0 (not corrected for isotope effects). Correlated spectroscopy (COSY) and nuclear Overhauser effect spectroscopy (NOESY) were acquired with pulsed field gradients (*31, 32*). Total correlation spectroscopy (TOCSY) was acquired according to Griesinger et al. (*33*). The typical size of a spectrum was 2048 × 400 with 64−128 scans for each experiment. NOESY spectra were acquired with two different mixing times (100 and 250 ms) to check for spin diffusion effects. All spectra were acquired at 289 K. NMR spectra were processed using nmrPipe and nmrDraw software (*34*). All spectra were zero-filled once in both dimensions, and 90° and 75° sine square window functions were applied to the F_2 and F_1 dimensions, respectively, before Fourier transformation. Proton chemical shifts were referenced to DSS (2,2-dimethyl-2-silapentane-5-sulfonate) as 0 ppm. Carbon-13 and nitrogen-15 chemical shifts were referenced indirectly to DSS by applying the converting ratios $^{13}C/^1H = 0.251449530$ and $^{15}N/^1H = 0.101329118$ as suggested by Wishart et al. (*35*). The chemical shifts for amino acids in a random coil state were taken from Wishart and Sykes (*36*).

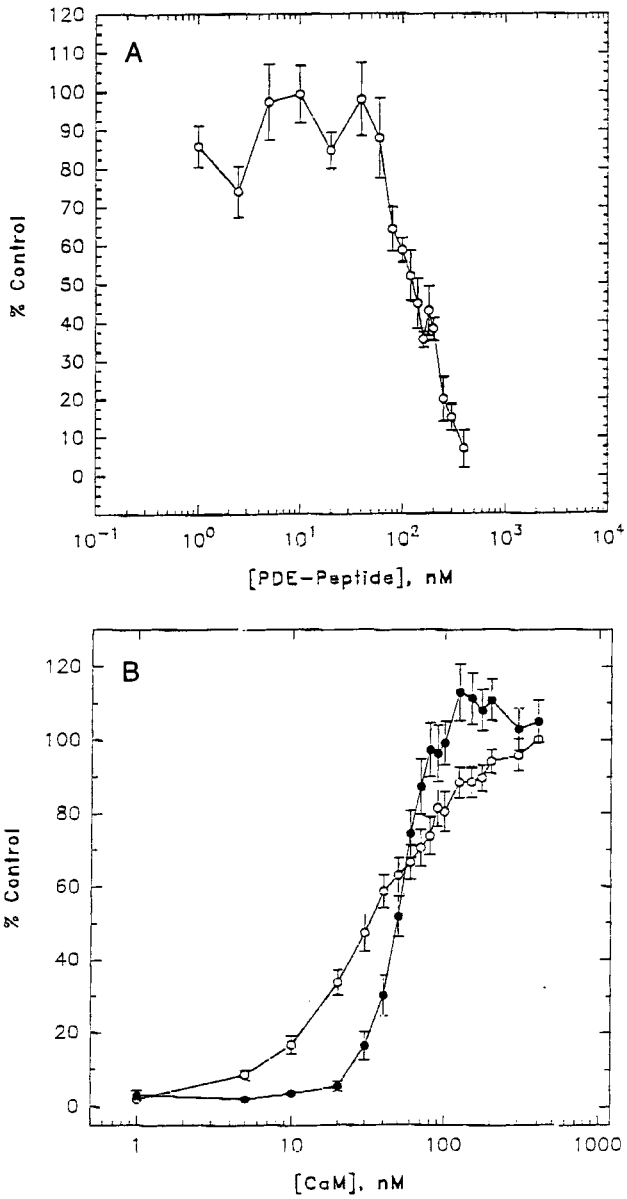

FIGURE 1: (A) Concentration-dependent inhibition of smMLCK by the PDE peptide in the presence of 100 nM Ca^{2+}-CaM (average of three experiments). (B) Activation curves of smMLCK by Ca^{2+}-CaM in the absence (empty circle, average of four experiments) or the presence (filled circle, average of six experiments) of 140 nM PDE peptide.

The α-Helical Content Prediction of Peptides. The α-helical content of peptides was calculated using the Agadir program that is available on the web site of the European Molecular Biology Laboratories (EMBL) in Heidelberg (*37*).

RESULTS

MLCK Assays. Figure 1A shows the concentration-dependent inhibition of smMLCK by the PDE peptide, the synthetic peptide corresponding to the CaM-binding domain

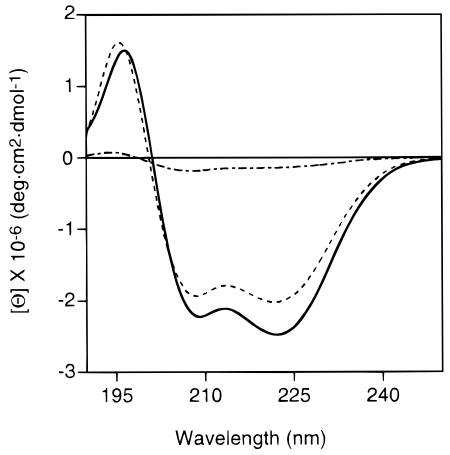

FIGURE 2: Far-UV CD spectra of the PDE peptide (dashed/dotted line), Ca^{2+}-CaM (dashed line), and the Ca^{2+}-CaM-PDE peptide complex (solid line). The CD intensities are expressed as the molar ellipticity.

of PDE1A2, in the presence of 100 nM CaM. Half-maximal inhibition was observed at ~110 nM peptide. The K_d for the PDE peptide binding to CaM was determined to be 224 nM, from the CaM activation curves in Figure 1B, which were determined in the absence and presence of 140 nM PDE peptide.

CD Spectroscopy. We examined the changes in the secondary structure of the CaM-PDE peptide complex by far-UV CD spectroscopy. The PDE peptide itself contains a small amount of α-helix. In the presence of Ca^{2+}, adding the PDE peptide to Ca^{2+}-CaM increases the negative molar ellipticity at both 208 and 222 nm (Figure 2). Difference CD spectra (not shown) confirm that α-helical structure is induced. Since Ca^{2+}-CaM usually does not gain any secondary structure in Ca^{2+}-CaM-peptide complexes (*10*−*12*), the increase in ellipticity of the complex can be attributed to the secondary structure of the bound peptide. Thus the PDE peptide binds to Ca^{2+}-CaM in an α-helical conformation. This is confirmed by isotope-filtered Fourier transform infrared (FTIR) spectroscopy (see below). The α-helical content of the bound PDE peptide is approximately 70%, as calculated from difference CD spectra (*27*). The inhibition of Ca^{2+}-CaM activation of MLCK by the PDE peptide probably results therefore from the competitive binding of the α-helical portion of the PDE peptide to Ca^{2+}-CaM. In this way, the CaM-binding domain of MLCK is displaced and MLCK remains in the autoinhibited state.

Since Charbonneau et al. (*15*) showed by steady-state Trp fluorescence that the PDE peptide also binds to CaM in the absence of Ca^{2+}, we studied the apo-CaM-PDE peptide interaction by far-UV CD spectroscopy. As shown in Figure 3A, the PDE peptide increases the negative ellipticity of apo-CaM at both 208 and 222 nm. However, the increase at 208 nm is smaller than that at 222 nm, giving rise to a difference spectrum that is not indicative of an α-helix (Figure 3B). Instead, the difference spectrum suggests a combination of α-helical and *β*-sheet/*β*-turn conformations (Figure 3B). If we assume that apo-CaM does not change its secondary structure significantly when bound to a target peptide, the difference spectrum can be attributed to the peptide bound to apo-CaM. The only well-characterized complex of a peptide with apo-CaM is for neuromodulin, and the results

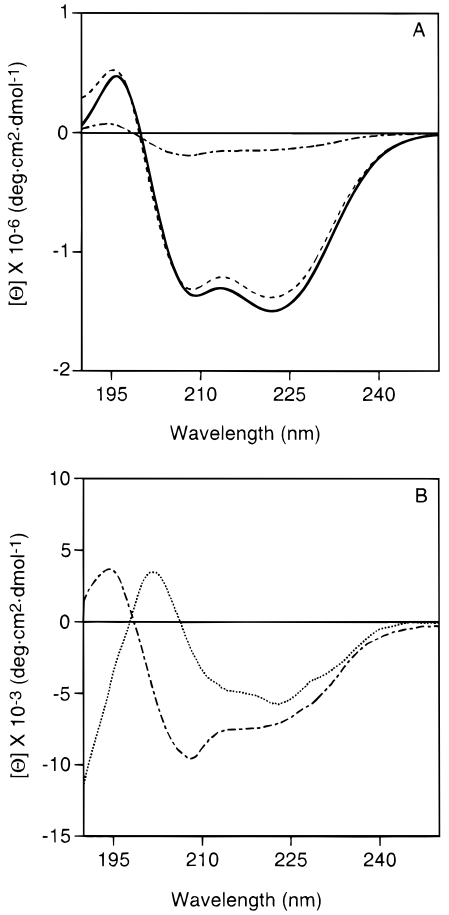

FIGURE 3: (A) Far-UV CD spectra of the PDE peptide (dashed/dotted line), apo-CaM (dashed line), and the apo-CaM-PDE peptide complex (solid line). The CD intensities are expressed as the molar ellipticity. (B) Far-UV CD spectrum of the PDE peptide (dashed/dotted line) and the difference spectrum between the apo-CaM-PDE peptide complex and apo-CaM (dotted line). The CD intensities are expressed as the mean residue molar ellipticity.

obtained suggest that this assumption is probably valid (*38*). Moreover, difference FTIR spectra (see below) show that there are no changes in the secondary structure of apo-CaM (and calcium CaM) upon peptide binding. Isotope-filtered FTIR spectroscopy of the apo-CaM-PDE peptide complex also detected two different peaks for the bound PDE peptide; one can be attributed to an α-helical conformation and the other to a *β*-sheet/*β*-turn conformation (see below).

Next we studied the conformation of the PDE peptide with increasing amounts of trifluoroethanol (TFE). TFE/aqueous solutions have been shown to stabilize the secondary structure of peptides, especially α-helices (*39*). The PDE peptide has ~22% α-helix in aqueous solution (Figure 4A), similar to the 16% predicted by the Agadir program (*37*). In the TFE titration, we observed an increase of the α-helical content of the PDE peptide, leveling off at ~20% TFE (Figure 4B). The PDE peptide contains ~47% α-helix in 60% TFE/H_2O. These TFE titration experiments indicate that the PDE peptide has the propensity to form an α-helix, as do most CaM-binding domain peptides (*39*).

While far-UV CD spectra are useful to assess the secondary structure of proteins and peptides, near-UV CD spectra can reveal changes in the tertiary structure of the aromatic residues of proteins. In the Ca^{2+}-CaM-PDE peptide complex, we observed significant changes in the near-UV CD spectrum

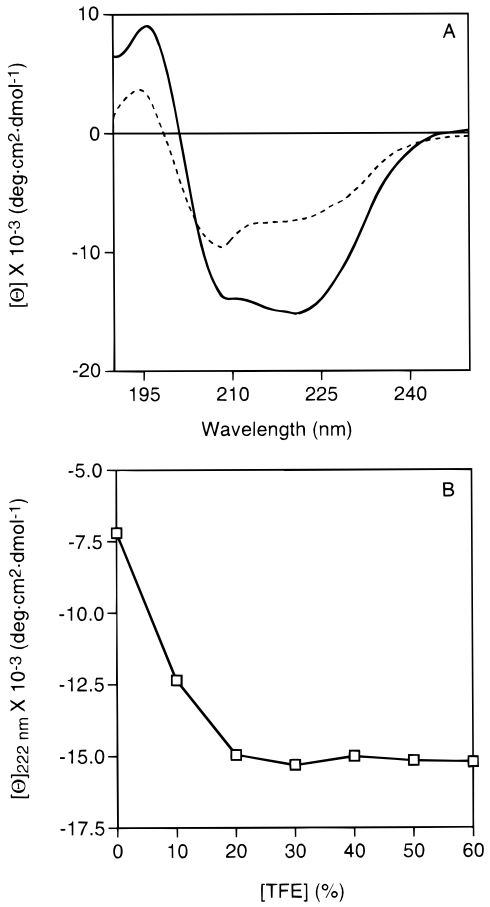

FIGURE 4: (A) Far-UV CD spectra of the PDE peptide in the absence (dashed line) and in the presence (solid line) of 60% TFE. (B) The TFE titration curve of the PDE peptide. The CD intensities in both figures are expressed as the mean residue molar ellipticity.

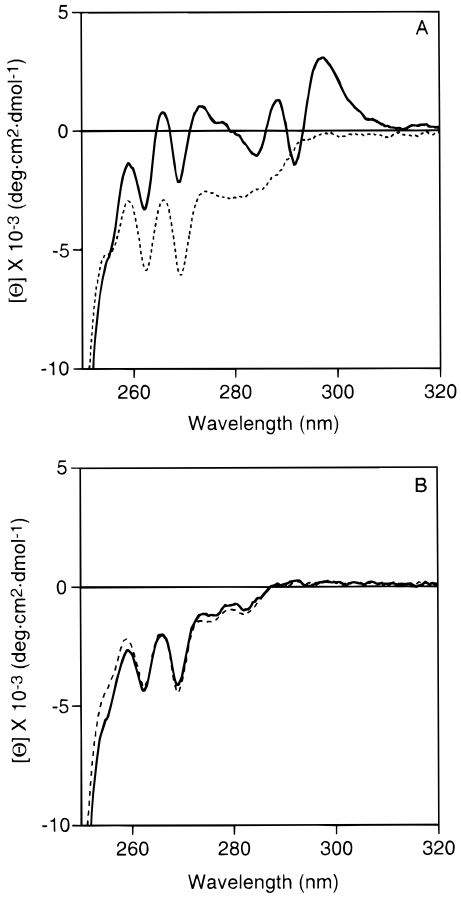

FIGURE 5: Near-UV CD spectra of Ca^{2+}-CaM (A) and apo-CaM (B) in the absence (dashed line) and presence (solid line) of the PDE peptide at 1:1 ratio. The CD intensities are expressed as the molar ellipticity. Note the positive bands around 288 and 297 nm in the Ca^{2+}-CaM-PDE peptide complex (A) originating from the sole Trp residue in the PDE peptide. In contrast, these two bands do not appear in the spectrum of the apo-CaM-PDE peptide complex (B).

of the complex compared with that of Ca^{2+}-CaM. The near-UV CD spectrum of the PDE peptide itself does not have any obvious features (data not shown). In the spectrum of the Ca^{2+}-CaM-PDE peptide complex, the bands around 263 and 269 nm arise from the eight Phe residues in CaM (there are no Phe residues in the PDE peptide), indicating the involvement of the Phe residues in Ca^{2+}-CaM in the complex formation (Figure 5A). The positive bands around 288 and 297 nm arise from the sole Trp residue in the PDE peptide (there are no Trp residues in CaM) (Figure 5A). These Trp bands are quite similar to the Trp bands in the near-UV CD spectra of the Ca^{2+}-CaM-MLCK peptide complex and the Ca^{2+}-CaM-CaMKI peptide complex (ref *40*, Gomes and Vogel, unpublished results). The positive Trp bands in the near-UV CD spectrum of the CaM-peptide complex are usually associated with a positive ^1L_a electronic transition, which occurs when the Trp residue in the peptide interacts predominantly with the C-terminal lobe of Ca^{2+}-CaM (*41*). Indeed, both MLCK peptide and CaMKI peptide bind to Ca^{2+}-CaM with the Trp in the N-terminal of the peptide interacting with the C-terminal lobe of Ca^{2+}-CaM (refs *10*, *11*, *22*, and Yuan and Vogel, unpublished results). Our near-UV CD spectra suggest that the PDE peptide adopts a similar orientation when bound to Ca^{2+}-CaM (Figure 5A). This binding orientation was further supported by steady-state Trp fluorescence measurements (see below). In the absence of Ca^{2+}, the near-UV CD spectrum of apo-CaM showed few changes upon addition of the PDE peptide (Figure 5B). Neither the Phe residues of CaM nor the single Trp residue of the PDE peptide, therefore, appears to be a major participant in the apo-CaM-PDE peptide interaction. This observation may be related to the relatively weak affinity of the PDE peptide for apo-CaM and the dynamic nature of the binding (see below).

FTIR Spectroscopy. To obtain further information about the secondary structure of the PDE peptide, we employed FTIR spectroscopy to study the secondary structure of the bound PDE peptide in the CaM-PDE peptide complexes. FTIR is an excellent method to study the secondary structure of proteins and peptides, since the position of the amide I band is diagnostic for different secondary structures (*42*). However, the amide I bands from proteins and peptides overlap in a protein-peptide complex. Zhang et al. (*21*) demonstrated that the amide I band of uniformly ^{13}C-labeled CaM shifts by 55 cm^{-1} to a lower wavenumber and thus leaves a clear window between 1640 and 1670 cm^{-1} for observation of the unlabeled bound peptide conformation in CaM-peptide complexes. In this study, we have employed this technique to study the CaM-PDE peptide complex in the absence and presence of Ca^{2+}. The PDE peptide in aqueous solution displays an amide I band centered around 1645 cm^{-1}; its position and half-bandwidth indicate the presence of random coil and α-helix conformation, which

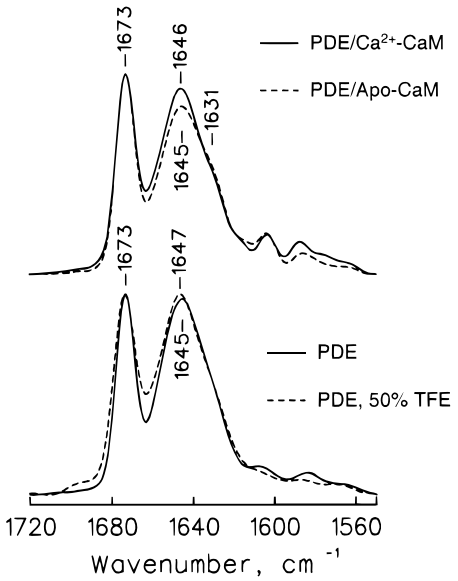

FIGURE 6: FTIR spectra of the free PDE peptide in aqueous solution and in 50% TFE aqueous solution (lower panel). Difference FTIR spectra of the PDE peptide in complex with Ca^{2+}-CaM and apo-CaM (upper panel). The spectra of the peptide in the complex were obtained by subtracting the spectrum of free $^{13}C/^{15}N$-labeled CaM from the spectrum of the corresponding $^{13}C/^{15}N$-labeled CaM/PDE peptide complex. The intense band at 1673 cm^{-1} is from the carry-over counterion trifluoroacetic acid (TFA) used in the peptide synthesis, and this band has been used to normalize the FTIR spectra acquired under different conditions. All spectra are shown after band-narrowing by Fourier self-deconvolution using a half-bandwidth of 16 cm^{-1} and a band-narrowing factor of 1.6.

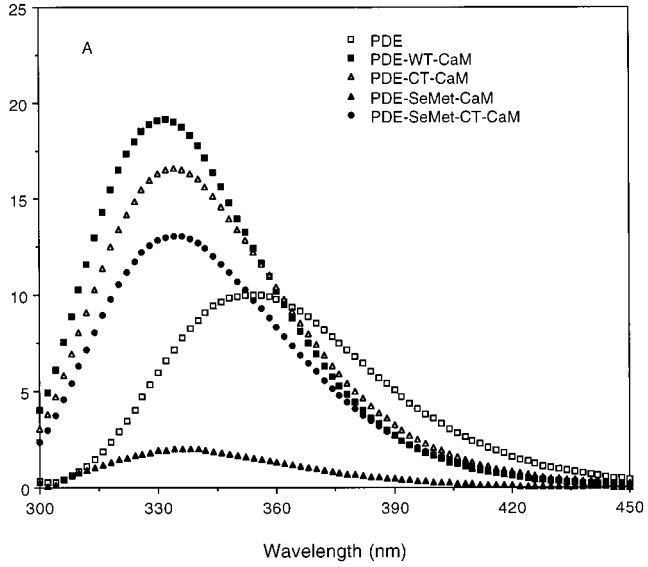

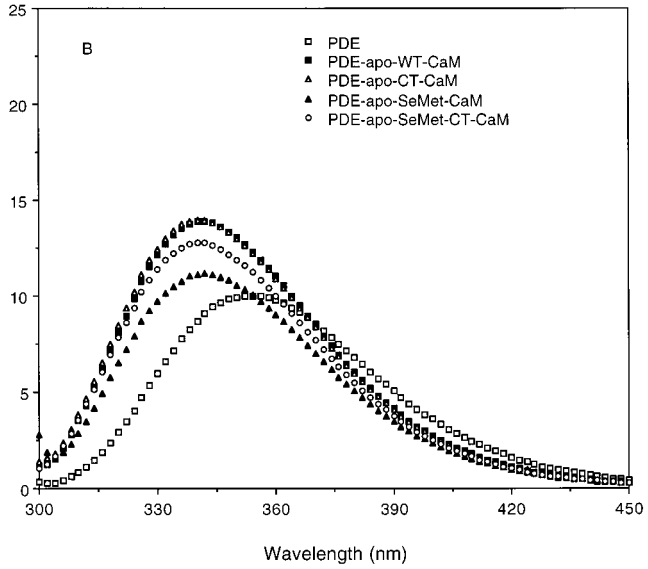

FIGURE 7: Steady-state Trp fluorescence spectra of the PDE peptide (empty square), the WT-CaM-PDE peptide complex (filled square), the CT-CaM-PDE peptide complex (empty triangle), the SeMet-CaM-PDE peptide complex (filled triangle), and the SeMet-CT-CaM-PDE peptide complex (filled circle). The fluorescence spectra were recorded in the presence of 1 mM $CaCl_2$ (A) or 5 mM EDTA (B). The concentrations used were 10 μM for the PDE peptide and 15 μM for all proteins. The protein concentration used is sufficient to saturate the PDE peptide (data not shown). See also Ohki et al. (*32*).

is consistent with the CD data (ref *42*, Figure 6 and Figure 4A). The FTIR spectrum of the PDE peptide in 50% TFE/D_2O solution displays a more typical α-helix conformation with an amide I band centered at 1647 cm^{-1} (Figure 6). Upon binding to apo-CaM, a broader amide I band is observed (Figure 6) and the peak intensity at 1646 cm^{-1} is reduced in comparison to the PDE peptide in aqueous solution. Furthermore, a shoulder at 1631 cm^{-1} as a new spectral feature is observed. The feature at 1631 cm^{-1} can be associated with the presence of β-sheet/β-turn structures, which are usually observed between 1625 and 1640 cm^{-1} (*42*). Thus, the infrared data of the PDE peptide bound to apo-CaM correlate with the far-UV data (Figure 3B), suggesting that α-helical and β-turn conformations are coexisting in the PDE peptide bound to apo-CaM. Finally, when the PDE peptide is bound to Ca^{2+}-CaM, a single band at 1646 cm^{-1} is observed in the FTIR spectrum (Figure 6), consistent with an ordered α-helical structure in the PDE peptide when bound to Ca^{2+}-CaM. Altogether, the results obtained by isotope-edited FTIR spectroscopy are fully consistent with those derived from CD spectroscopy.

Finally, it should be noted that there are no large difference spectroscopic features in the range 1560−1615 cm^{-1} (upper panel of Figure 6). Possible differences in this region would indicate a conformational difference between free CaM and CaM complexed with the PDE peptide, because the spectra given in the upper panel of Figure 6 were obtained by subtracting the spectrum of free $^{13}C/^{15}N$-labeled CaM from that of the labeled protein in complex with the peptide. The fact that the difference spectroscopic features in the range 1560−1615 cm^{-1} (upper panel of Figure 6) are very similar to the weak infrared bands already observed for the free PDE peptide in this region (lower panel of Figure 6) demonstrates that there are virtually no changes in the secondary structure of CaM upon binding to the peptide. This holds for both the apo- and the Ca^{2+}-bound form of the PDE-CaM complex.

Fluorescence Spectroscopy. Since the PDE peptide contains a single Trp residue and CaM does not possess any Trp residues, we can use Trp fluorescence to follow the peptide binding to CaM. Four different CaM variants were used to determine the peptide-binding orientation in the Ca^{2+}-CaM-PDE peptide complex (*22*). The steady-state Trp fluorescence of the PDE peptide displays a maximum emission wavelength at 353 nm (Figure 7A), which is typical for a solvent-exposed Trp residue. When Ca^{2+}-WT-CaM was added, a significant increase of the Trp fluorescence quantum

yield and a 22 nm blue shift of the maximum emission wavelength (to 331 nm) were observed (Figure 7A). This suggests that the Trp residue in the PDE peptide becomes buried in a hydrophobic environment when bound to Ca^{2+}-CaM. These results are in agreement with those reported by Charbonneau et al. (*15*) and Ohki et al. (*28*). When we added Ca^{2+}-CT-CaM, a CaM mutant with four Met residues in the C-lobe of CaM (M109, M124, M144, and M145) mutated to Leu residues (*24*), a small decrease of the fluorescence intensity was observed in the complex (Figure 7A). If the Trp is bound to the N-terminal lobe of Ca^{2+}-CT-CaM, the intact N-terminal lobe of CT-CaM should not change the fluorescence of the Trp residue in the PDE peptide. If the Trp residue is bound to the C-terminal lobe of Ca^{2+}-CT-CaM, mutation of four Met residues in the C-terminal lobe of CaM to Leu residues could have given rise to an increase of the Trp fluorescence intensity, because the mutations have removed the fluorescence-quenching ability of the sulfur atoms of Met residues (*22*). Obviously, this was not observed; however, the Trp residue of the PDE peptide probably does bind to the C-terminal lobe of Ca^{2+}-CaM (see below). We propose that the small decrease in Trp fluorescence in the Ca^{2+}-CT-CaM-PDE peptide complex arises from a structural rearrangement in the complex, imposed by the four mutations. Subsequently, we studied a complex of SeMet-CaM and the PDE peptide. The significant decrease in the Trp fluorescence suggests that the Trp residue of the PDE peptide binds to one of the two hydrophobic patches of Ca^{2+}-SeMet-CaM, because the efficient quenching properties of the selenium atoms almost completely abolish the Trp fluorescence (ref *22*, Figure 7A). Finally, we used SeMet-CT-CaM, a CaM variant with the four Met residues in the N-terminal lobe of CaM (M36, M51, M71, and M72) substituted by SeMet and the four Met residues in the C-terminal lobe of CaM (M109, M124, M144, and M145) mutated to Leu residues (*22*). The fluorescence spectrum obtained with this variant confirms that the Trp residue in the PDE peptide binds to the C-terminal lobe of CaM; the Trp fluorescence intensity would have been much lower if the Trp binds to the N-terminal lobe of Ca^{2+}-SeMet-CT-CaM which possesses the SeMet residues (ref *22*, Figure 7A). Overall, our steady-state fluorescence spectroscopy results suggest an antiparallel orientation when the PDE peptide binds to Ca^{2+}-CaM.

In the absence of Ca^{2+}, binding of apo-WT-CaM to the PDE peptide rendered a 12 nm blue shift and a slight increase of the fluorescence quantum yield (Figure 7B), as also observed by Charbonneau et al. (*15*). Similar spectra were obtained when apo-CT-CaM, apo-SeMet-CaM, and apo-SeMet-CT-CaM bound the PDE peptide (Figure 7B). The less dramatic changes observed in these fluorescence spectra for the apo-CaM complex, when compared to the calcium-CaM complex, suggest that the Trp residue in the PDE peptide is bound in a less hydrophobic environment when bound to apo-CaM, consistent with our near-UV CD spectra (Figure 5B). Moreover, the absence of substantial Trp fluorescence quenching by SeMet residues (Figure 7B) suggests that the Met residues are not directly involved in binding the Trp residue in apo-CaM.

NMR Spectroscopy. The interaction between Ca^{2+}-CaM and PDE peptide has been studied previously in our laboratory and others (*15*, *24*, *28*). Zhang et al. (*24*) reported that the PDE peptide can form a 1:1 high-affinity complex

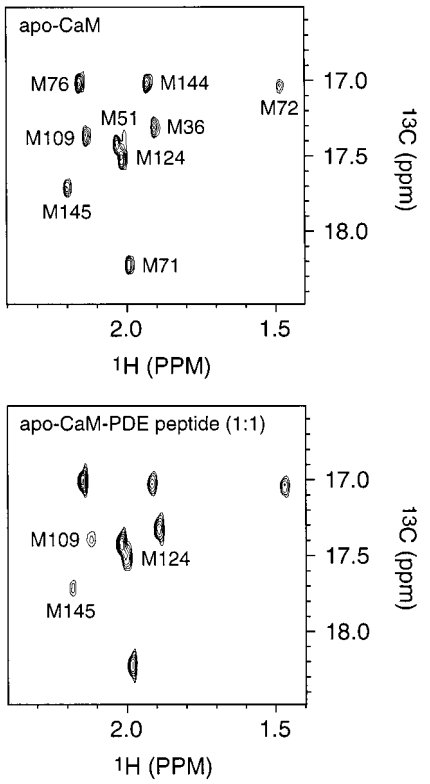

FIGURE 8: Two-dimensional ^1H, ^{13}C HMQC NMR spectra of the methyl groups of the Met residues in apo-CaM and in a 1:1 ratio complex of apo-CaM and the PDE peptide. Note the broadening effects of M109, M124, and M145 of apo-CaM in the presence of the PDE peptide.

with Ca^{2+}-CaM and that all eight Met residues in both lobes of Ca^{2+}-CaM are involved in the peptide binding. Since fluorescence, far-UV CD, and FTIR spectroscopy showed that the PDE peptide also interacts with apo-CaM (Figures 3, 6, and 7B), we characterized this interaction by NMR spectroscopy. When the PDE peptide was titrated into ^{13}C-methyl-Met-labeled CaM in the absence of Ca^{2+}, we observed almost no chemical shift changes (Figure 8). Instead, the methyl resonances of M109, M124, and M144 in the ^1H, ^{13}C HMQC spectra broadened during the titration (Figure 8), indicating that the binding of the PDE peptide to apo-CaM is relatively weak and involves chemical exchange processes. Interestingly, all of the broadened peaks are from the C-terminal lobe of apo-CaM while those from the N-terminal lobe of apo-CaM are unaffected (Figure 8). We further mapped global resonance changes in the apo-CaM-PDE peptide complex using ^{15}N uniformly labeled CaM. Similar to the ^{13}C-methyl-Met-labeled CaM, ^1H, ^{15}N HSQC spectra of apo-CaM showed significant broadening effects in the spectra with little chemical shift changes accompanying the addition of the PDE peptide (Figure 9). Again we found that many resonances are too broad to be observed in the 1:1 apo-CaM-PDE peptide complex and all of these are from the C-terminal lobe of CaM (Figure 9, the broadened residues are all labeled in the figure). Both NMR titration experiments therefore indicate that the PDE peptide binds to the C-terminal lobe of apo-CaM, although we cannot totally exclude the possibility that some residues in the N-terminal lobe of apo-CaM are also involved in the interaction. Unfortunately the exchange process involves residues from many different regions in the C-terminal lobe of apo-CaM,

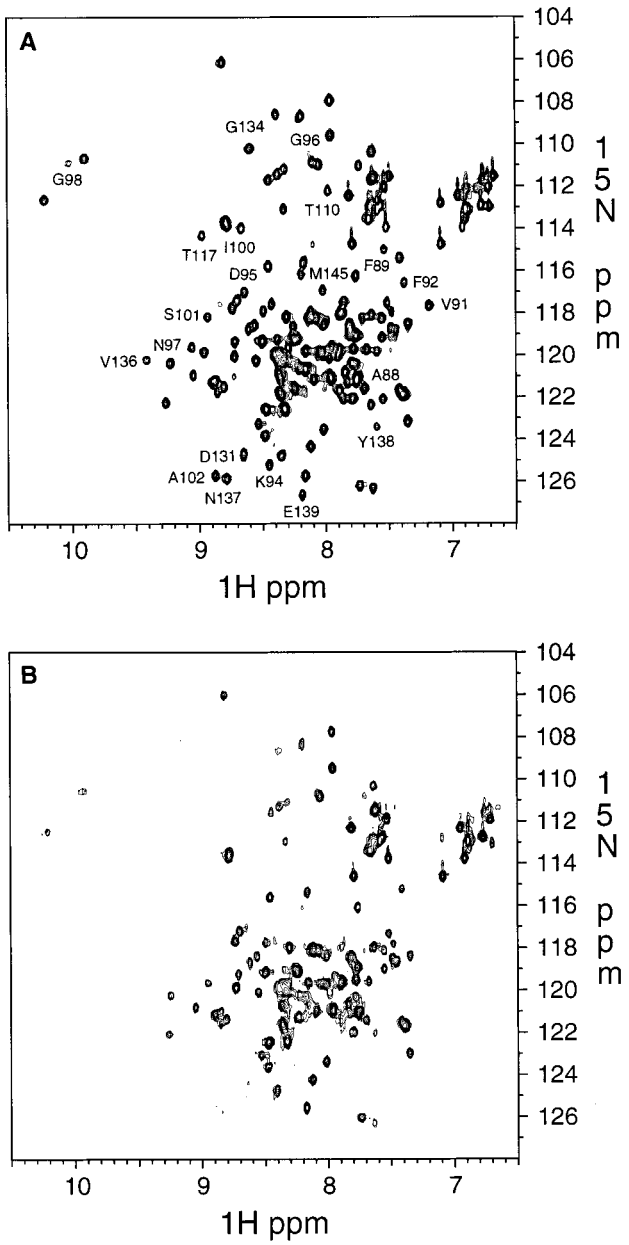

FIGURE 9: Two-dimensional ^{1}H, ^{15}N HSQC NMR spectroscopy of apo-CaM (A) and the 1:1 ratio complex of apo-CaM and the PDE peptide (B). Some resonances have been labeled in the spectrum of apo-CaM, and these correspond to those resonances which are too broad to detect in the spectrum of the complex in the well-resolved region. For the NMR assignment of apo-CaM, see Ohki et al. (*32*).

suggesting that it reflects an overall conformational change for this lobe rather than specific broadening at the site of peptide binding. This makes it impossible to pinpoint a specific region for the binding of the PDE peptide on apo-CaM. Attempts to determine the structure of the PDE peptide bound to apo-CaM by transfer nuclear Overhauser effects (TrNOE) spectroscopy were also not successful, because the chemical exchange phenomena led to resonances that were too broad to be studied productively (data not shown, Figure 9).

The ^{1}H NMR spectra of the PDE peptide in 30% aqueous TFE have been completely assigned, and the nOe and the secondary chemical shifts are summarized in Figure 10. The continuous strong $NN_{(i,\ i+1)}$ connections and the many $\alpha N_{(i,\ i+3)}$, $\alpha N_{(i,\ i+4)}$, and $\alpha\beta_{(i,\ i+3)}$ medium-range nOe's suggest an α-helical structure from residue Lys4 to residue Leu20 in the PDE peptide in 30% TFE/aqueous solution (Figure 10). The upfield-shifted α-proton chemical shifts and the downfield-shifted α-carbon chemical shifts also support the formation of an α-helix in the PDE peptide in the TFE aqueous solution (ref *36*, Figure 10). These NMR data are consistent with the results obtained by far-UV CD and FTIR spectroscopy in the presence of TFE (Figures 4 and 6).

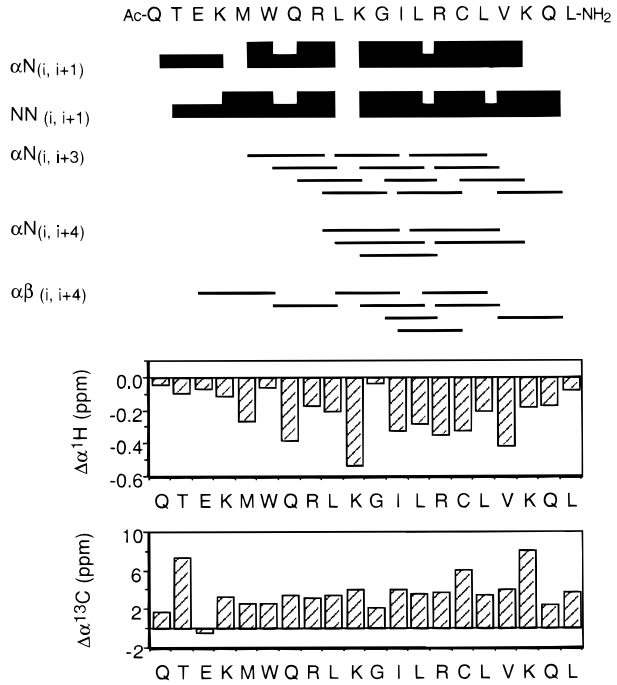

FIGURE 10: The nOe summary and the α-proton and α-carbon chemical shift deviations of the PDE peptide in 30% TFE aqueous solution.

DISCUSSION

The far-UV CD spectroscopy results show that the PDE peptide binds to Ca^{2+}-CaM with an α-helical structure (Figure 2). Isotope-filtered infrared spectroscopy also supports the notion that the PDE peptide forms an α-helix when bound to Ca^{2+}-CaM (Figure 6). This is a normal binding mode for the interaction of CaM-binding domains of target proteins with Ca^{2+}-saturated CaM (*10*−*12*). Since the MLCK peptide also binds to Ca^{2+}-CaM with an α-helical structure (*10*, *11*), the PDE peptide is expected to compete with MLCK for Ca^{2+}-CaM; this effect is illustrated by MLCK activity competition assays (Figure 1). We note that the PDE peptide also binds to Ca^{2+}-CaM in an antiparallel orientation, as indicated by the near-UV CD spectroscopy and steady-state Trp fluorescence results (Figures 5 and 7A). The same binding orientation has been found for most CaM-binding domain peptides studied to date (*10*−*12*, *22*). Finally, Zhang et al. (*24*) showed that the eight Met residues from both lobes of Ca^{2+}-CaM are involved in the binding of the PDE peptide; again this is also the case for other well-studied CaM-peptide complexes (*43*). Thus the binding mode of the PDE peptide to Ca^{2+}-CaM resembles that of other well-characterized almost globular Ca^{2+}-CaM-peptide complexes, such as the Ca^{2+}-CaM-MLCK peptide complex and the Ca^{2+}-CaM-CaMKII peptide complex (*10*−*12*), where the peptide interacts with hydrophobic regions on both domains, leading to a compaction of the overall CaM structure.

In the absence of Ca^{2+}, the PDE peptide binds to apo-CaM in a conformation that is only partially α-helical and probably contains β-turns (Figures 3 and 6). The difference CD spectroscopy and isotope-filtered FTIR spectroscopy gave complementary and consistent results when we used both approaches to determine the peptide conformation bound to CaM (Figures 3 and 6). The binding of apo-CaM to the PDE peptide resembles the only well-characterized apo-CaM-peptide interaction, that of the apo-CaM-neuromodulin peptide complex. The neuromodulin peptide also adopts an α-helix when bound to apo-CaM, as demonstrated by NMR and CD spectroscopy (*44*−*46*); moreover, it mainly interacts with the C-terminal lobe of CaM (*38*). Thus the apo-CaM-PDE peptide complex represents a related interaction mode for apo-CaM and a CaM-binding domain peptide. In contrast, we have shown recently by difference far-UV CD spectroscopy that the iNOS peptide binds to apo-CaM in a type II β-turn, which is distinct from the neuromodulin peptide and the PDE peptide (*47*). Titrations of apo-CaM with the PDE peptide reveal that the methyl groups of the Met residues in the C-terminal lobe of apo-CaM are significantly broadened, but no changes in their chemical shifts are detected. In contrast, the Met methyl groups of the N-terminal lobe of apo-CaM with the PDE peptide do not experience any perturbations. Titration of uniformly ^{15}N-labeled apo-CaM further confirmed that the perturbations are restricted to the C-terminal lobe of apo-CaM, since all of the severely broadened resonances in the well-resolved region of the spectra are from the C-terminal lobe of apo-CaM. These titration experiments strongly suggest that the PDE peptide only interacts with the C-terminal lobe of apo-CaM. The C-terminal lobe of apo-CaM adopts a partially opened conformation whereas the N-terminal lobe of apo-CaM is completely closed (*43*, *48*).

A number of studies have shown that Trp residues in CaM-binding domains usually prefer to bind to the hydrophobic cleft of the C-terminal lobe of Ca^{2+}-CaM. When anchored in this position, the bound Trp side chain gives rise to characteristic near-UV CD spectra (*40*, *41*); the fluorescence of such a Trp can be effectively quenched by the Met and SeMet residues of calcium-CaM, because of the close approach of the sulfur and selenium atoms to the indole ring (*22*). In our studies, the single Trp residue of the PDE peptide binds in the expected manner to the C-terminal lobe of Ca^{2+}-CaM, giving rise to similar near-UV CD and fluorescence-quenching spectra as the MLCK and CaMKI peptides (refs *22*, *40*, *41*, and Gomes and Vogel, unpublished results). However, the results obtained for the apo-protein clearly show that the Trp residue does not play a similar pivotal role in the binding to apo-CaM. In fact the near-UV CD results (Figure 5B) even suggest that the Trp residue does not maintain a stable tertiary structure when bound to apo-CaM. Also the fluorescence data show that the Trp fluorescence is not quenched significantly by binding to apo-SeMet-CaM (Figure 7B); this demonstrates that the Met side chains are not directly involved in Trp binding (*22*), consistent with the idea that they are not solvent-exposed in apo-CaM. Consequently, Trp interacts with other residues in apo-CaM, explaining in part the reduced blue shift and fluorescence quantum yield compared to calcium-CaM (Figure 7). Clearly insertion of the Trp indole ring into the hydrophobic cleft of the C-terminal lobe of Ca^{2+}-CaM appears to play a major role in the Ca^{2+} activation mechanism of PDE. We suggest that this is the initial binding step followed by induction of α-helical structure throughout the peptide, which then binds to both domains of CaM and leads to the compaction of the overall complex structure as observed for MLCK and CaMKll (*10*−*12*). However solution X-ray scattering studies show that not all CaM-binding peptides or combinations thereof (e.g., phosphorylase kinase and plasma membrane calcium-pump) give rise to such a compacted complex structure (*49*, *50*), indicating that there may be different modes for CaM-target interactions.

In this study, we have discovered that the PDE peptide adopts two distinct conformations when bound to Ca^{2+}-CaM or apo-CaM. This is a novel finding that illustrates the flexibility that exists in some CaM-binding domains. Indeed, in X-ray studies the CaM-binding domains from calcineurin and adenylyl cyclase do not have well-defined electron densities in the crystals of intact protein, probably due to their flexibility (*51*, *52*). In another CaM target protein, CaM-dependent protein kinase I, the structure of the CaM-binding domain in the autoinhibited enzyme is well-defined. However, only part of this region has an α-helical structure (*53*). Combined with the present study, we suggest that lack of a regular secondary structure might be a common feature in most CaM-binding domains. The subsequent induction of regular α-helical structures in these regions by binding to Ca^{2+}-CaM is probably an important component of the enzyme activation mechanism.

Recent studies have shown that, besides the main CaM-binding domain peptide studied here, a second region of PDE1 further downstream (approximately 90 residues) also binds tightly to Ca^{2+}-CaM (*54*). Phosphorylation of Ser120 in this part of PDE1A2 by cyclic AMP-dependent protein kinase reduces its affinity for Ca^{2+}-CaM (*55*). Further studies with longer peptides or intact protein are required to elucidate in more detail the interactions between CaM and PDE. Nevertheless, our studies are insightful in understanding the interactions between CaM and a group of target proteins that can bind to CaM in the absence and presence of Ca^{2+}, for example, PDE1A1 (*56*), inducible nitric oxide synthase (*47*, *57*), phosphorylase kinase (*58*), adenylyl cyclase (*59*), and neuromodulin (*38*, *44*−*46*).

REFERENCES

1. Vogel, H. J. (1994) *Biochem. Cell Biol. 72*, 357−376.
2. Crivici, A., and Ikura, M. (1995) *Annu. Rev. Biophys. Biomol. Struct. 24*, 85−116.
3. Vogel, H. J., and Zhang, M. (1995) *Mol. Cell. Biochem. 149/150*, 3−15.
4. Ikura, M. (1996) *Trends Biochem. Sci. 21*, 14−17.
5. Babu, Y. S., Bugg, C. E., and Cook, W. J. (1988) *J. Mol. Biol. 204*, 191−204.
6. Kuboniwa, H., Tjandra, N., Grzesiek, S., Ren, H., Klee, C. B., and Bax, A. (1995) *Nat. Struct. Biol. 2*, 768−776.
7. Zhang, M., Tanaka, T., and Ikura, M. (1995) *Nat. Struct. Biol. 2*, 758−767.
8. Barbato, G., Ikura, M., Kay, L. E., Pastor, R. W., and Bax, A. (1992) *Biochemistry 31*, 5269−5278.
9. O'Neil, K. T., and DeGrado, W. F. (1990) *Trends Biochem. Sci. 15*, 59−64.
10. Ikura, M., Clore, G. M., Gronenborn, A. M., Zhu, G., Klee, C. B., and Bax, A. (1992) *Science 256*, 632−638.
11. Meador, W. E., Means, A. R., and Quiocho, F. A. (1992) *Science 257*, 1251−1255.

12. Meador, W. E., Means, A. R., and Quiocho, F. A. (1993) *Science 262*, 1718−1721.
13. Gellman, S. H. (1991) *Biochemistry 30*, 6633−6636.
14. Beavo, J. A. (1995) *Physiol. Rev. 75*, 725−748.
15. Charbonneau, H., Kumar, S., Novack, J. P., Blumenthal, D. K., Griffin, P. R., Shabanowitz, J., Hunt, D. F., Beavo, J. A., and Walsh, K. A. (1991) *Biochemistry 30*, 7931−7940.
16. Yan, C., Zhan, A. Z., Bently, J. K., and Beavo, J. A. (1996) *J. Biol. Chem. 271*, 25699−25706.
17. Walsh, M. P., Valentine, K. A., Ngai, P. K., Carruthers, C. A., and Hollenberg, M. D. (1984) *Biochem. J. 224*, 117−127.
18. Ngai, P. K., Carruthers, C. A., and Walsh, M. P. (1984) *Biochem. J. 218*, 863−870.
19. Zhang, M., and Vogel, H. J. (1993) *J. Biol. Chem. 268*, 22420−22428.
20. Zhang, M., and Vogel, H. J. (1994) *Biochemistry 33*, 1163−1171.
21. Zhang, M., Fabian, H., Mantsch, H. H., and Vogel, H. J. (1994) *Biochemistry 33*, 10883−10888.
22. Yuan, T., Weljie, A. M., and Vogel, H. J. (1998) *Biochemistry 37*, 3187−3195.
23. Bárány, K., and Bárány, M. (1996) in *Biochemistry of Smooth Muscle Contraction* (Bárány, M., Ed.) pp 21−35, Academic Press, San Diego, CA.
24. Zhang, M., Li, M., Wang, J. H., and Vogel, H. J. (1994) *J. Biol. Chem. 269*, 15546−15552.
25. Allen, B. G., Andrea, J. E., and Walsh, M. P. (1994) *J. Biol. Chem. 269*, 29288−29298.
26. Erickson-Viitanen, S., and DeGrado, W. F. (1987) *Methods Enzymol. 139*, 455−478.
27. Scholtz, J. M., Qian, H., York, E. J., Stewart, J. M., and Baldwin, R. (1991) *Biopolymers 31*, 1463−1470.
28. Ohki, S., Ikura, M., and Zhang, M. (1997) *Biochemistry 36*, 4309−4316.
29. Bax, A., Griffey, R. H., and Hawkins, B. L. (1983) *J. Magn. Reson. 55*, 301−315.
30. Wider, G., and Wüthrich, K. (1993) *J. Magn. Reson., Ser. B 102*, 239−241.
31. Davis, A. L., Laue, E. D., Keeler, J., Moskau, D., and Lohman, J. (1991) *J. Magn. Reson. 94*, 637−644.
32. Jeener, J., Meier, H., Bachman, P., and Ernst, R. R. (1979) *J. Chem. Phys. 71*, 4546−4553.
33. Griesinger, C., Otting, G., Wüthrich, K., and Ernst, R. R. (1988) *J. Am. Chem. Soc. 110*, 7870−7872.
34. Delaglio, F., Grzesiek, S., Vuister, G. W., Zhu, G., Pfeifer, J., and Bax, A. (1995) *J. Biomol. NMR 6*, 277−293.
35. Wishart, D., Bigam, C. G., Yao, J., Abildgaard, F., Dyson, H. J., Oldfield, E., Markley, J. L., and Sykes, B. D. (1995) *J. Biomol. NMR 6*, 135−140.
36. Wishart, D. S., and Sykes, B. D. (1994) *Methods Enzymol. 239*, 363−392.
37. Muñoz, V., and Serrano, L. (1997) *Biopolymers 41*, 495−509.
38. Urbauer, J. L., Short, J. H., Dow, L. K., and Wand, A. J. (1995) *Biochemistry 34*, 8099−8109.
39. Zhang, M., Yuan, T., and Vogel, H. J. (1993) *Protein Sci. 2*, 1931−1937.
40. Findlay, W. A., Martin, S. R., Beckingham, K., and Bayley, P. M. (1995) *Biochemistry 34*, 2087−2094.
41. Barth, A., Martin, S. R., and Bayley, P. M. (1998) *Biopolymers 45*, 493−501.
42. Jackson, M., and Mantsch, H. H. (1995) *Crit. Rev. Biochem. Mol. Biol. 30*, 95−120.
43. Yuan, T., Ouyang, H., and Vogel, H. J. (1999) *J. Biol. Chem.* (in press).
44. Zhang, M., Vogel, H. J., and Zwiers, H. (1994) *Biochem. Cell Biol. 72*, 109−116.
45. Urbauer, J. L., Ehrhardt, M. R., Bieber, R. J., Flynn, P. F., and Wand, A. J. (1996) *J. Am. Chem. Soc. 118*, 11329−11330.
46. Gerendasy, D. D., Herron, S. R., Jennings, P. A., and Sutcliffe, J. G. (1995) *J. Biol. Chem. 270*, 6741−6750.
47. Yuan, T., Vogel, H. J., Sutherland, C., and Walsh, M. P. (1998) *FEBS Lett. 431*, 210−214.
48. Swindells, M. B., and Ikura, M. (1996) *Nat. Struct. Biol. 3*, 501−504.
49. Trewhella, J., Blumenthal, D. K., Rokop, S. E., and Seeger, P. A. (1990) *Biochemistry 29*, 9316−9324.
50. Kataoka, M., Head, J. F., Vorherr, T., Krebs J., and Carafoli, E. (1991) *Biochemistry 30*, 6247−6251.
51. Kissinger, C. R., Parge, H. E., Knighton, D. R., Lewis, C. T., Pelletier, L. A., Tempczyk, A., Kalish, V. J., Tucker, K. D., Showalter, R. E., Moomaw, E. W., Gastinel, L. N., Habuka, N., Chen, X., Maldonado, F., Barker, J. E., Bacquet, R., and Villafranca, J. E. (1995) *Nature 378*, 641−644.
52. Zhang, G., Liu, Y., Ruoho, A. E., and Hurley, J. H. (1997) *Nature 386*, 247−253.
53. Goldberg, J., Nairn, A. C., and Kuriyan, J. (1996) *Cell 84*, 875−887.
54. Sonnenburg, W. K., Seger, D., Kwak, K. S., Huang, J., Charbonneau, H., and Beavo, J. A. (1995) *J. Biol. Chem. 270*, 30989−31000.
55. Florio, V. A., Sonnenburg, W. K., Johnson, R., Kwak, K. S., Jensen, G. S., Walsh, K. A., and Beavo, J. A. (1994) *Biochemistry 33*, 8948−8954.
56. Sharma, R. K., and Wang, J. H. (1986) *J. Biol. Chem. 261*, 14160−14166.
57. Cho, H. J., Xie, Q.-W., Calaycay, J., Mumford, R. A., Swiderek, K. M., Lee, T. D., and Nathan, C. (1992) *J. Exp. Med. 176*, 599−604.
58. Dasgupta, M., Honeycutt, T., and Blumenthal, D. K. (1989) *J. Biol. Chem. 264*, 17156−17163.
59. Ladant, D. (1988) *J. Biol. Chem. 263*, 2612−2618.

BI9816453